International Journal of Microwave and Wireless Technologies

cambridge.org/mrf

Linearity metrics of pre-matched AlGaN/GaN RF transistor: multi-tone simulation and measurement analysis

José Anderson Silva Dos Santos[1], Julien Alleman[1], Margot Leventoux[1], Pierre Medrel[1], Christophe Chang[2], Raphael Sommet[1], Fabien Courrèges[1] and Jean-Christophe Nallatamby[1]

[1]University of Limoges, XLIM, France and [2]United Monolithic Semiconductors SAS, France

Research Paper

Cite this article: Silva Dos Santos JA, Alleman J, Leventoux M, Medrel P, Chang C, Sommet R, Courrèges F, Nallatamby J-C (2026) Linearity metrics of pre-matched AlGaN/GaN RF transistor: multi-tone simulation and measurement analysis. *International Journal of Microwave and Wireless Technologies*, 1–10. https://doi.org/10.1017/S1759078726103699

Received: 31 December 2025 UTC
Revised: 12 July 2026 UTC
Accepted: 15 July 2026 UTC

Keywords:
ACPR; GaN HEMT; linearity characterization; matching networks; microwave measurements; multi-tone characterization; PAE; power amplifiers; pre-matched transistor; USMT

Corresponding author:
José Anderson Silva Dos Santos;
Email:
jose_anderson.silva_dos_santos@xlim.fr

Abstract

The present work provides a comprehensive analysis of non-linear distortions using Unequally Spaced Multi-Tone (USMT) signals under realistic modulated operating conditions. The investigation focused on USMT stimuli with 2, 4, and 6 tones, with the objective to assess large-signal performance of a pre-matched GaN HEMT device at 29 GHz manufactured by United Monolithic Semiconductors. Experimental measurements were conducted on-wafer and compared with nonlinear Harmonic Balance simulations, incorporating electromagnetic models for passive elements and the manufacturer's design kit for active components. Furthermore, continuous-wave load-pull simulations were conducted to assess the optimal load impedance for maximum power-added efficiency (PAE). The findings indicate that increasing the number of tones results in a substantial decrease in drain current density due to trapping effects, along with a concomitant degradation in PAE. A corresponding reduction in adjacent channel power ratio (ACPR) was also observed, and an analytical relationship between ACPR and the number of tones was derived. The strong agreement between simulated and measured ACPR values serves to confirm the accuracy of the modelling approach and to validate the reliability of the measurement setup.

Introduction

The objective of modern wireless communication systems is to address the growing demand for enhanced data transmission rates and increased utilization of the available spectral resources. In order to address these issues, current and future telecommunication standards are exploring higher frequencies and more complex modulation schemes, such as Orthogonal Frequency Division Multiplexing (OFDM). These signals are characterized by Gaussian statistical properties and a high peak-to-average power ratio (PAPR) [1–4], leading to new challenges for the modelling and characterization of the front-end of radiofrequency systems. In this regard, the power amplifier (PA) constitutes a pivotal element of the microwave emitter. Indeed, it is the component that remains the dominant consumer of energy. Consequently, the primary objective of PA designers is to optimize transistor performance for a specific operating point.

While conventional characterization methods relying on continuous wave or two-tone stimuli provide fundamental insights into large-signal performances, they fail to adequately capture the device's behavior under realistic operating conditions involving wideband, high-PAPR signals [1–4]. For this reason, the utilization of complex signals in the characterization of PAs has become an increasingly prevalent practice. For instance, the utilization of a multi-tone signal, characterized by bandwidth and statistical properties analogous to those of 5 G waveform standards, exemplifies this approach. The best linear approximation framework was employed to estimate the error vector magnitude (EVM) of the amplifier without IQ demodulation [5–8].

The Unequally Spaced Multi-Tones (USMT) signal was selected to characterize the linearity and performance of the devices under test (DUT). Due to the statistical properties of this signal, such as the probability density function (PDF) and the complementary cumulative distribution function (CCDF), it is analogous to complex modulation signals when the number of carriers is minimal [4, 9–11]. Furthermore, the non-equidistance of signal frequencies enables the discernment of the original signal's frequencies from those of the intermodulation products, as they do not coincide with the signal carriers or other intermodulation products [4]. This approach enables the separate measurement of the components using the PNA-X spectrum analyzer function. Another feature is that the PAPR of the signal is independent of the phase

© The Author(s), 2026. Published by Cambridge University Press in association with The European Microwave Association.

Downloaded from https://www.cambridge.org/core. UNIVERSIDAD AUTONOMA METROPOLITANA, on 17 Nov 2026 at 04:20:28, subject to the Cambridge Core terms of use, available at https://www.cambridge.org/core/terms. https://doi.org/10.1017/S1759078726103699

of each of the carriers [10]. The statistical properties of USMT signals can be adjusted based on the number of signal carriers and the amplitude and phase of each carrier. These parameters are tunable, allowing the generation of a signal that accurately emulates the characteristics of the reference complex modulated waveform. However, a USMT signal with a cumulative distribution function analogous to that of the modulated signal will not invariably possess the same PAPR [4]. A significant challenge in this field pertains to the selection of an appropriate signal. This procedure is governed by several criteria, such as frequency spacing, amplitude, and phase of the carriers, and is contingent upon the specific requirements of the intended application. A methodology employing specific frequency tone planning as in a study by Angelotti and Gibiino [12] has been developed to achieve a low time-bandwidth product, thereby minimizing the time required to characterize nonlinear systems.

These signal characteristics are crucial for accurately capturing the non-linear behavior of the PA. As PAs typically achieve maximum efficiency in the saturated region, operating in this regime inherently compromises linearity. Therefore, evaluating the trade-off between efficiency and linearity specifications using realistic signals, such as USMT, is essential to ensure compliance with communication standards. To this end, the established equivalence between linearity merit factors, specifically EVM and noise power ratio (NPR), under dense, noise-like excitation conditions (typical of OFDM signals) has paved the way for advanced measurement setups. This work utilizes a measurement bench based on a PNA-X network analyzer [10, 13–18], exploiting this equivalence to perform accurate characterization. In essence, the performance of the PA is predominantly determined by its transistors. Therefore, rigorous characterization of these components is imperative to derive valid models for effective PA design.

Power transistors are far from 50 Ω; therefore, it is necessary to transform the system impedance to source and load impedances when the transistor operates with a large signal in order to optimize power performance, such as maximum efficiency or maximum output power. The source-pull and load-pull methods play a central role in identifying these optimal impedances. By systematically varying the source and load impedances, one can observe the nonlinear behavior of transistors in relation to performance metrics such as output power, efficiency, and linearity.

It is crucial to recognize that the input and output impedances generated by impedance matching networks exhibit frequency-dependent variations in response to the applied signal. Consequently, for a broadband signal, the input and output impedances between the lower and upper edges of the signal spectrum can result in a significant impedance shift. Consequently, the design of matching networks must ensure that the impedances presented remain within the acceptable range of the desired bandwidth. It is imperative to utilize simulations and measurements to comprehend the influence of electromagnetic (EM) effects, losses, and other factors on impedance transformation, as this can lead to discrepancies between the simulated and measured performance of the PA. A combination of nonlinear simulation and EM simulation is typically employed [19, 20].

Expanding upon preliminary findings presented at the European Microwave Week 2025 [21], the objective of this work is to characterize the nonlinear behavior of transistors for a USMT signal with 2 (USMT-2, which is the classical two-tone signal), 4 (USMT-4), and 6 (USMT-6) carriers. Experimental measurements were performed using a power device with input and output matching networks (OMNs) (pre-matched), supplied by the United Monolithic Semiconductors (UMSs) foundry. Subsequently, a comparison is made between the experimental results and the simulations performed using the design kit provided by the transistor manufacturer. The objective of this comparison is to evaluate the consistency between the experimental results and the simulations.

Description of the USMT signal and the linearity figures of merit

In order to characterize the intermodulation effects created by the nonlinearity of the device, it is necessary to use a multi-carrier signal. Two-tone signals do not allow observation of some effects that occur when a traditional complex signal, such as OFDM-encoded signals, is applied.

The proposed signal for characterizing the devices is the USMT signal. The most important characteristic of this signal is the absence of overlap between the intermodulation products and the signal carriers. This configuration enables the measurement of the power of each signal tone and intermodulation tone products, allowing for a discrete assessment of each signal component. Equation (1) enables the calculation of the signal's frequencies.

$$f_k = f_0 + \Delta f \cdot (k-1) + p_k \cdot f_{\in} \tag{1}$$

In this equation, f_0 indicates the frequency of the first signal carrier, Δ_f is the spacing between carriers, and $p_k \cdot f_{\in}$ represents extra spacing between frequencies in order to avoid frequency overlap. $f_{\in}$ is the frequency resolution of the fast Fourier transform.

Relevant features are the statistical properties of the utilized signals, including the PDF and the CCDF. This facilitates the comparison of USMT signals with digitally modulated carriers. Figure 1 shows the PDF and CCDF of the USMT-2, USMT-4, and USMT-6 signals, which have 2, 4, and 6 frequency tones, respectively.

It is shown that the more signal carriers are used, the more the PDF of the signal I(t) (in-phase) or Q(t) (in quadrature) is closer to a Gaussian distribution [9]. As a result, signals using the OFDM modulation scheme have a Gaussian-shaped PDF for the signals I(t) and Q(t). It is also noteworthy that CCDF facilitates the observation of the PAPR. For a USMT signal and under the assumption that all carriers have an identical amplitude, the PAPR of the signal is governed by equation (2), as illustrated in Fig. 1(b) [10, 22].

$$\mathrm{PAPR}\,(dB) = 10 \cdot \log(\mathrm{N}) \tag{2}$$

Consequently, the PAPR of the signal escalates with the number of signal carriers, thereby constraining the linear operating range of the transistor.

Adjacent channel power ratio (ACPR) is an important figure of merit for non-linear device characterization. It is defined as the ratio between the power of the main channel, the relevant part of the output signal, to the power in the adjacent channels due to the intermodulation products generated by the device [23]. Given the absence of overlap between the intermodulation products, as illustrated in Fig. 2, the ACPR can be calculated by measuring the power at each of the frequencies located in the adjacent channels and in the main channel (signal carriers).

The ACPR for a USMT signal can be delineated through equation (3).

$$\mathrm{ACPR}\,(dB) = 10 \cdot \log\left(\frac{\sum_{f \in f_{\mathrm{carriers}}} P_{OUT}(f)}{\sum_{f \in f_{\mathrm{adjacents}}} P_{OUT}(f)}\right) \tag{3}$$

Downloaded from https://www.cambridge.org/core. UNIVERSIDAD AUTONOMA METROPOLITANA, on 17 Nov 2026 at 04:20:28, subject to the Cambridge Core terms of use, available at https://www.cambridge.org/core/terms. https://doi.org/10.1017/S1759078726103699

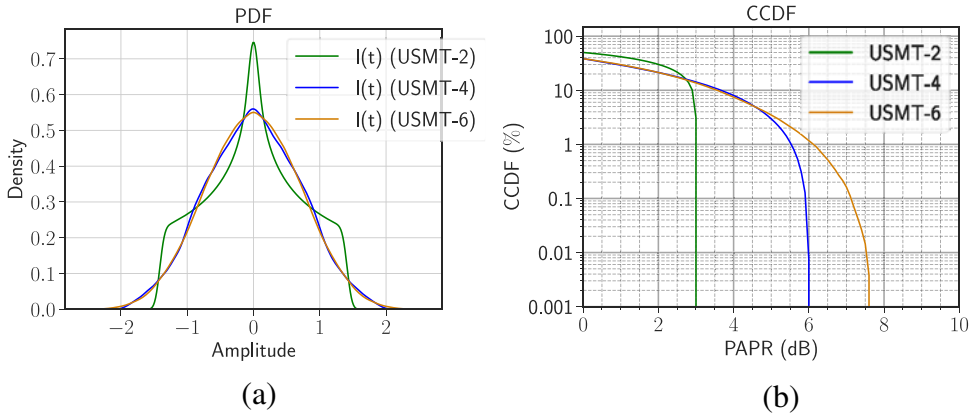


Figure 1. Statistical properties of the USMT-2 (2-Tones), USMT-4 and USMT-6 signals: (a) probability density function (PDF) of I(t); (b) complementary cumulative distribution function.

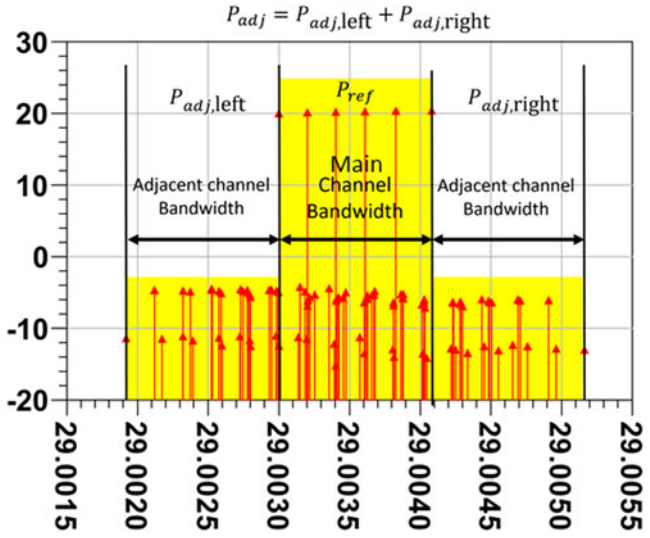


Figure 2. Definition of ACPR using USMT-6 signal.

In this equation, $f_{carriers}$ denotes the frequencies of the signal carriers, while $f_{adjacent}$ signifies the frequencies of the intermodulation products generated in the channels adjacent to the band of the signal of interest.

Methodology

The device under test examined in this study is a pre-matched (Input/Ouput) at 29 GHz that serves as a process validation circuit 8 × 50 µm GaN HEMT on a wafer from UMSs. As shown in Figure 3, the transistor is pre-matched at the input and at the output.

For a class AB quiescent point, the DC drain current (I_{DS0}) is set at approximately 150 mA/mm and the drain voltage (V_{DS0}) at 20 V. The operating frequency is 29 GHz.

The device was tested using various signals, including USMT-2, USMT-4, and USMT-6, to assess its performance under diverse conditions. A comparison between the simulated and measured behavior of the device is presented for each signal.

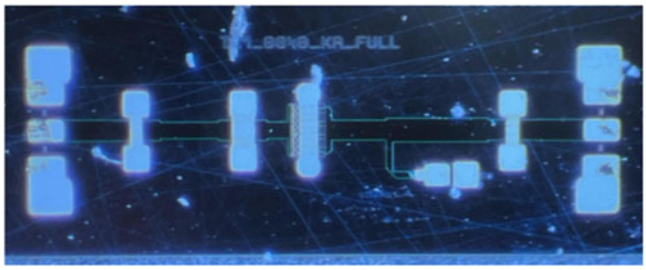


Figure 3. Detail of the UMS GH-15 pre-matched transistor.

Measurement setup

To characterize the transistor depicted in Figure 3, an on-probe measurement bench was developed and is illustrated in Figure 4. The test bench consists of a PNA-X, which is employed to measure the spectrum and power of the incident and reflected waves at the input and output of the DUT. The PNA-X N5245B vector network analyzer product from Keysight Technologies was used in this investigation.

In order to ascertain that the input and output power measurements are in the reference plane of the device indicated in blue (Fig. 4), a short-open-load-reciprocal on-probe calibration with an additional power calibration step was performed [24].

The Rohde & Schwarz SMW200A vector signal generator was used to create the signal under consideration. A characteristic feature of this instrument is its ability to generate signals with arbitrary waveforms at high frequencies.

USMT-2, USMT-4, and USMT-6 were the signals used to characterize the device; Table 1 lists their corresponding frequencies [25]. The signal bandwidth ranges from 201 kHz for the USMT-2 signal to 1.081 MHz for the USMT-8 signal, which indicates a narrowband signal.

The input range power is −10 dBm to 23 dBm. The transistor can operate in both the linear and saturation zones thanks to this range. As a result, the behavior of the transistor may be seen throughout these distinct operating zones.

Simulation process

In the context of simulation, it is of paramount importance to meticulously replicate the measurement conditions within the

Downloaded from https://www.cambridge.org/core. UNIVERSIDAD AUTONOMA METROPOLITANA, on 17 Nov 2026 at 04:20:28, subject to the Cambridge Core terms of use, available at https://www.cambridge.org/core/terms. https://doi.org/10.1017/S1759078726103699

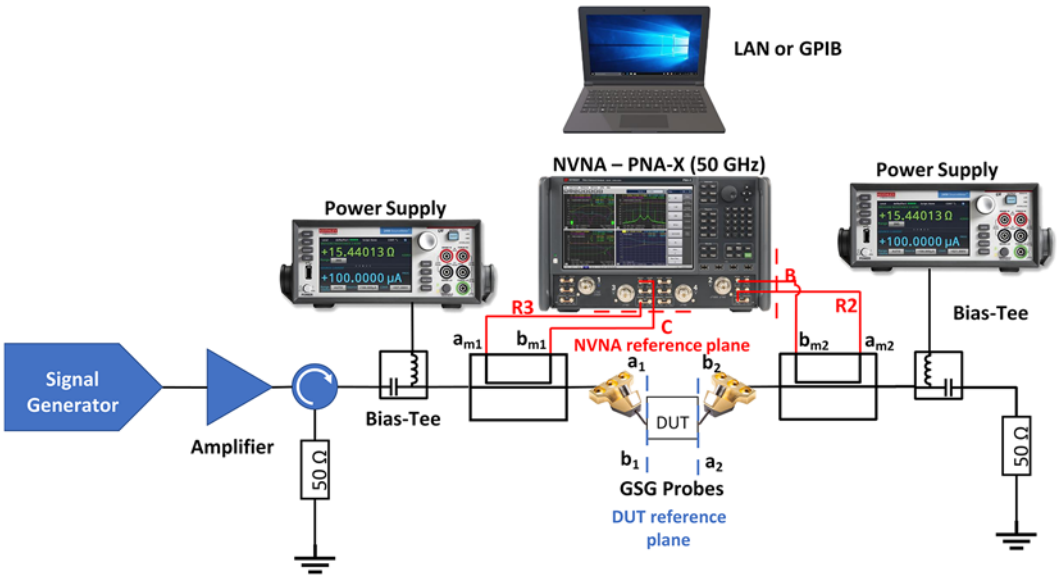


Figure 4. PNA-X-based measurement setup for measuring the PAE using a multi-tones signal.

Table 1. USMT signal freq. used to characterize the DUT

	Freq. (GHz)		Freq. (GHz)		Freq. (GHz)
f_1	29.003000	f_2	29.003201	f_3	29.003403
f_4	29.003609	f_5	29.003827	f_6	29.004081

Advanced Design System software. In order to achieve this, the transistor was simulated using the GH15 Design Kit supplied by UMS. Here, a GDS file was supplied by the foundry in order to simulate the tested device using an EM simulator. The schematic of this simulation is shown in Figure 5.

To achieve this, the input matching network (IMN) and OMN are simulated using the Momentum solver. The circuit was then simulated using the harmonic balance (HB) solver, and the nonlinear electrothermal model of the 8 × 50 µm component was updated with the S parameters of the IMN and OMN. Subsequently, the bias point was adjusted to reproduce the measurement conditions.

The S parameters of the simulated matching network were adjusted to match the results closer to the measured S parameters as a calibration step between the simulation and the measurements. In order to achieve this objective, a series of adjustments were implemented, including modifications to the active resistance of the transistor by using the spread parameters. This approach made it possible to simulate variances related to manufacturing and design processes. Another change involved modifying the electrothermal model's component temperature, which was required due to a lack of direct thermal measurements. Finally, to model some minor manufacturing or measurements errors related to the passive circuit, transmission lines of approximately 10 µm were added.

It is essential to carry out a comprehensive study of the matching network simulations before analyzing the outcomes of the pre-matched transistor combining the transistor and the matching networks. This entails observing the matching procedures performed by these networks. In order to accomplish this objective, the S parameters of the transistor for a continuous drain current $I_{DS0} = 60\ mA$ (which corresponds to 150 mA/mm for an 8 × 50 µm transistor) and the S parameters of the matching networks were simulated, as illustrated in Figure 6 (a) for frequencies between 25 and 30 GHz.

In the context of the IMN, impedance matching at the input stage is achieved through the presentation of the conjugate of S_{11} of the transistor. Thus, it is necessary to compare the S_{22} of the IMN with the conjugate of S_{11} of the transistor when the drain is loaded by an OMN + 50 Ω. It can be observed that the IMN is matched with the input impedance of the transistor.

A similar approach can be used to analyze the OMN (Fig. 6(b)). It is necessary to compare the S_{11} of the OMN with the conjugate of S_{22} of the transistor when the gate is loaded by an IMN + 50 Ω. The latter is particularly crucial for transistor performance since load impedance affects features such as gain and efficiency.

A thorough examination of the figure indicates that the impedance presented by the OMN does not correspond to an impedance match, as the OMN's S_{11} does not equate to the conjugate of the transistor's S_{22}. The OMN does not match the optimal power-added efficiency (PAE) value, according to a similar analysis of the output reflection coefficients at 29 and 30 GHz, which enable maximum PAE to be obtained.

It was thought that a load-null simulation analysis of this transistor would be significant because the device has not been matched to the load impedance and OMN prevents the achievement of maximal PAE. Consequently, the contours of the output power, gain, and PAE of this component can be observed in Figure 7.

It is important to note that the optimal points are not located in the center of the Smith charts. However, the greatest PAE value is around 39%, whereas a transistor without matching networks simulation allows a PAE above 45%. This discrepancy can be attributed to the occurrence of losses within the matching networks, which in turn leads to a reduction in the resulting power and total gain.

The DUT under consideration is a test pattern (process control monitoring – PCM), so the impedance matching is not as precise as it would be for a PA. The gain block is employed to verify the proper functioning of the process.

Following these characterizations, a secondary simulation using the S parameters shown in Figures 7 allows for the analysis of the

Downloaded from https://www.cambridge.org/core. UNIVERSIDAD AUTONOMA METROPOLITANA, on 17 Nov 2026 at 04:20:28, subject to the Cambridge Core terms of use, available at https://www.cambridge.org/core/terms. https://doi.org/10.1017/S1759078726103699

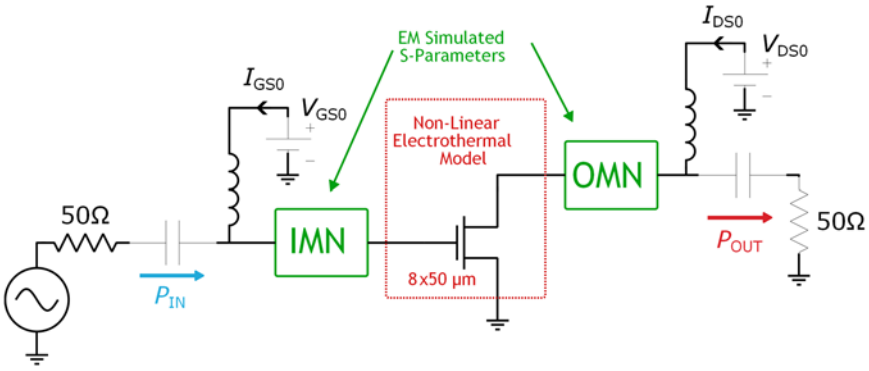


Figure 5. Schematic of the electromagnetic co-simulation and circuit of the pre-matched component.

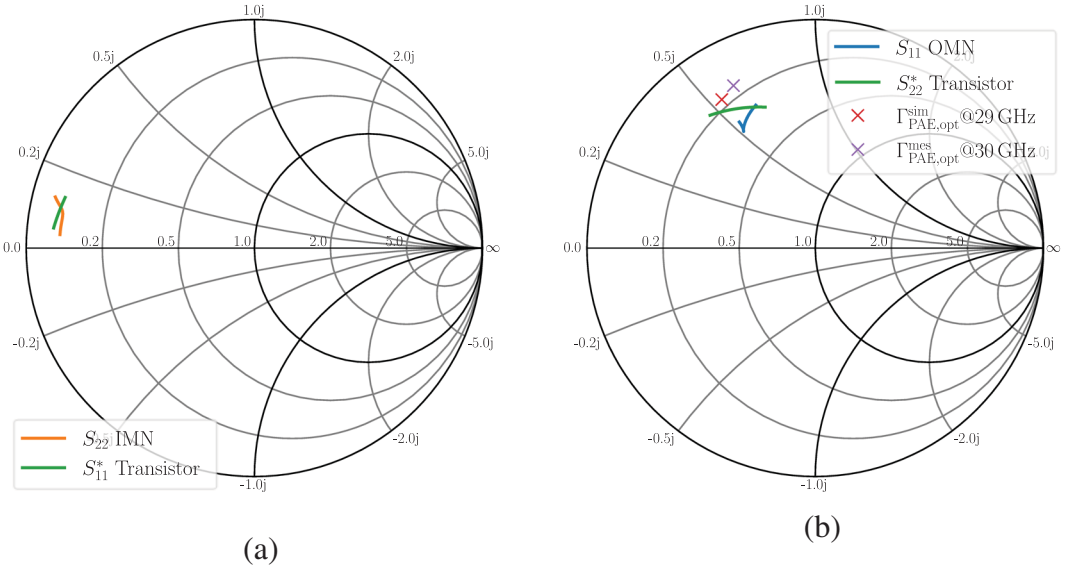


Figure 6. (a) Comparison between S_{22}^{IMN} and the conjugate of $S_{11}^{transistor}$. (b) Comparison between S_{11}^{OMN}, conjugate of, and optimal impedances for PAE at 29 and 30 GHz.

comprehensive circuit shown in Figure 4. Here, the HB simulation is used to incorporate third-order intermodulation products and harmonics. This simulation enables the observation of the nonlinear behavior of the device, a requirement for calculating the PAE. The simulation was executed by utilizing the USMT signals previously outlined, with a bias voltage of $V_{GS0} = -2.65\ V$, thereby yielding a drain bias current of approximately 60 mA. The input power is measured within the range of −10 to 30 dBm, a range designed to encompass the linear and nonlinear characteristics of the device.

Results

Transistors operate most efficiently when they are used close to their compression point. As illustrated in Figure 8, a comparison is made between the simulation and measurement of PAE utilizing USMT signals. The power values indicated in the following results correspond to their average values. The simulation of the USMT-2 signal demonstrates that for an output power of 29.5 dBm, a maximum PAE of 30.5% was obtained, and 29.5% for the measurement. An increase in the number of tones in the USMT signal necessarily implies a decrease in the maximum PAE value. For instance, the maximum PAE value obtained for the USMT-4 signal was 28.8% in the simulation and 28.2% in the measurement. For the USMT-6 signal, the maximum value obtained for the simulation was 28%, while the measurement yielded a maximum value of 26%.

The observed discrepancies between measurement and simulation results can be attributed to the inherent challenges in reproducing the precise measurement conditions within the simulation framework. These challenges become particularly pronounced when the device operates close to its compression point, the nonlinear region under a complex modulated signal, or when dealing with a high PAPR signal.

A comparative analysis was performed using the USMT-2 (shown in orange), USMT-4 (shown in green), and USMT-6 (shown in red) signals. The device was simulated (dashed lines) and measured (solid lines) for each signal. As illustrated in Figure 9, the output power is depicted as a function of the input power.

The results demonstrate that the device exhibits consistent behavior across all three signals, indicating that the gain and output power remain constant when an input power is applied during both simulation and measurement. However, a minor discrepancy emerges between the simulation and the measurement when the device operates within its linear range.

The average input power of the USMT-4 signal is constrained to a maximum value of $P_{in} \approx 24$ dBm and that of the USMT-6 signal is limited to $P_{in} \approx 21$ dBm. This is attributable to an increase in gate

Downloaded from https://www.cambridge.org/core. UNIVERSIDAD AUTONOMA METROPOLITANA, on 17 Nov 2026 at 04:20:28, subject to the Cambridge Core terms of use, available at https://www.cambridge.org/core/terms. https://doi.org/10.1017/S1759078726103699

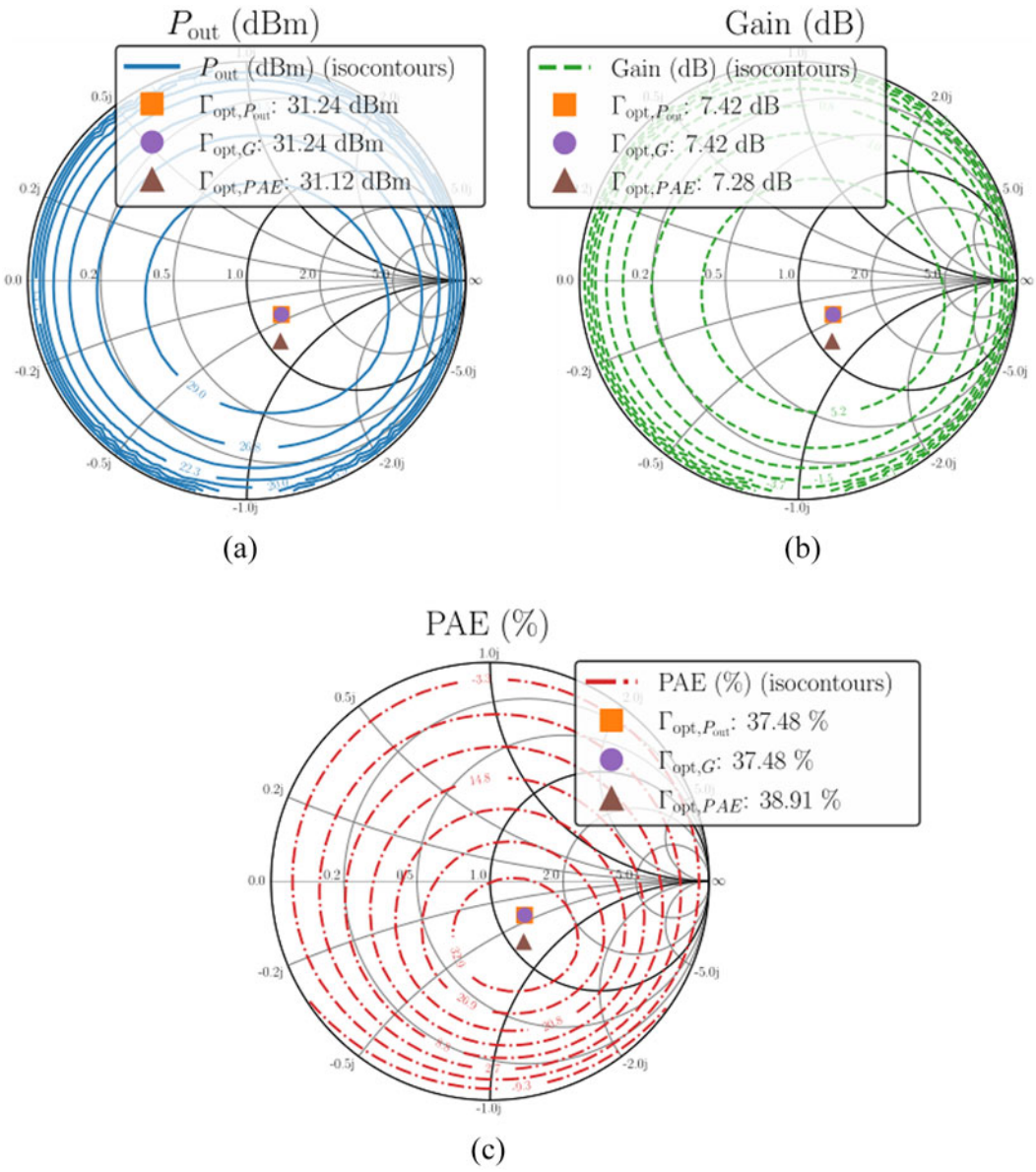


Figure 7. Load-pull contours at 30 GHz (pre-matched). Optimal points: P_{out} (square), gain (circle), and PAE (triangle).

current (I_G) caused by a higher maximum instantaneous power. It is imperative to note that increasing the input power beyond this point can result in transistor damage.

The analysis of the drain current depicted in Figure 10 reveals a degree of similarity among the various methods under consideration. In general, the drain current (I_D) remains around 60 mA when the device operates in its linear region. However, a decrease in drain current is observable when the output power is approximately 10–20 dBm. This decay is associated with an imbalance in the capture and emission processes of the trap charges, suggesting an increase in the charge state as the input power increases. This phenomenon is attributable to the asymmetric time constant of the traps, which is proportional to the instantaneous excursion of the drain voltage [26, 27].

The PAPR increases as the number of signal carriers increases, which in fact causes the current excursion to climb at a certain output power. This can be attributed to the increase in recovery time that occurs in conjunction with an increase in PAPR [27]. For an output power greater than 20 dBm, the drain current increases with similar dynamics for all signals.

The device does not exhibit a pronounced decrease in DC drain current as a function of RF signal power when the signal's PAPR is increased, because the device is a PCM whose output impedance matching does not result in load cycles with large voltage excursions. Such excursions are typically observed when the transistor operates near its efficiency optimum. Consequently, the DUT is not the optimally suitable option for demonstrating the effect of an increase in PAPR.

The existence of intermodulation products that do not overlap the signal carriers or other intermodulation products explains the use of the USMT signal in the nonlinear characterization of the transistor. The calculation of the ACPR is made by the analysis of the intermodulation products in the adjacent bands. As illustrated in Figure 11, a comparison is presented between the simulated and

Downloaded from https://www.cambridge.org/core. UNIVERSIDAD AUTONOMA METROPOLITANA, on 17 Nov 2026 at 04:20:28, subject to the Cambridge Core terms of use, available at https://www.cambridge.org/core/terms. https://doi.org/10.1017/S1759078726103699

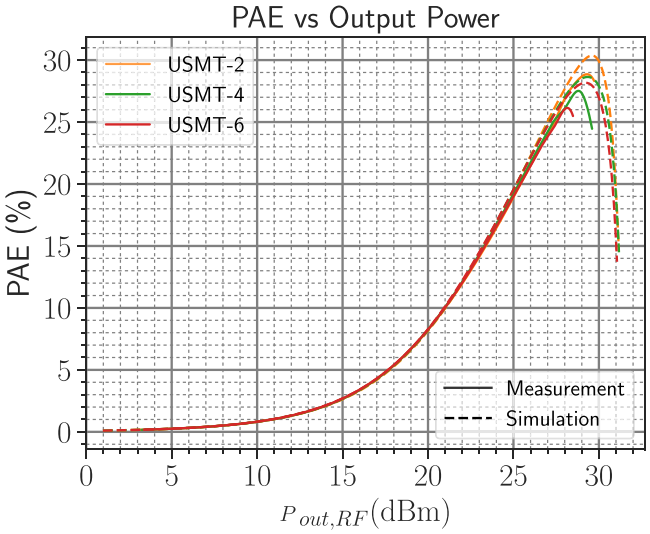


Figure 8. Simulated (dashed lines) and measured (solid lines) PAE vs output power for different USMT configurations.

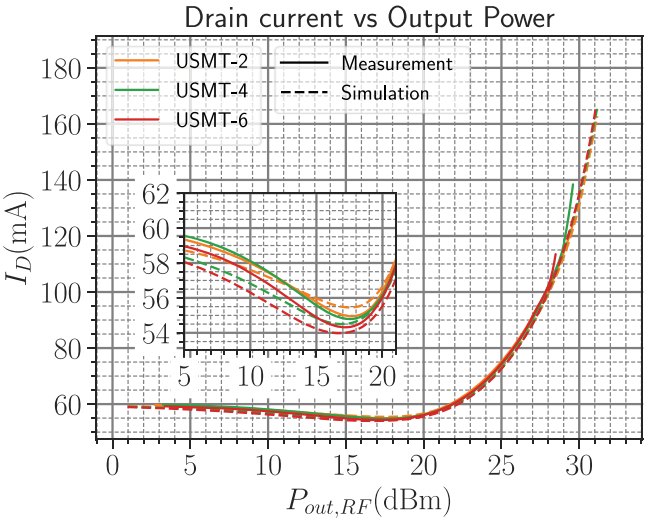


Figure 10. Comparison between simulation (dashed lines) and measurements (solid lines) of the DC drain current (I_D) consumption. A current drop is depicted in the inset.

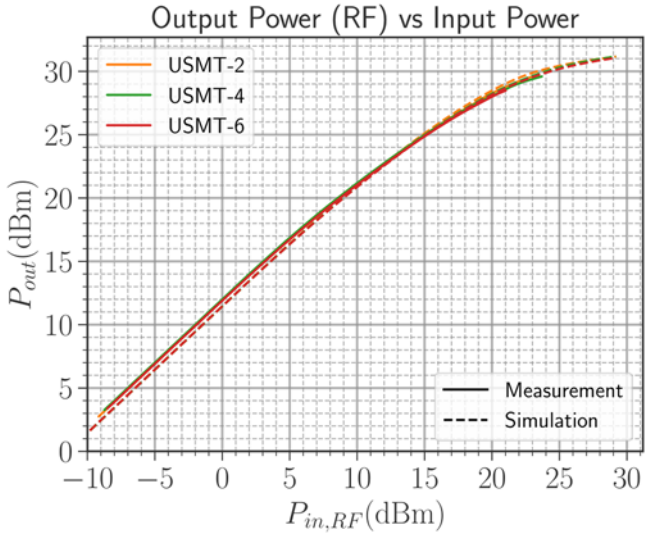


Figure 9. Comparison between simulation (dashed lines) and measurements (solid lines) of the output power.

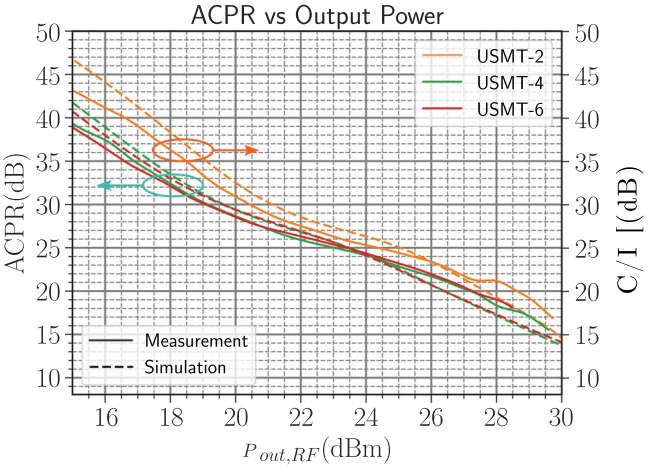


Figure 11. Simulated (dashed lines) and measured (solid lines) ACPR (4 and 6 tones) and C/I (2 tones) vs output power for different USMT configurations.

measured ACPR as a function of output power for various USMT signals.

A thorough examination of the simulations and measurements reveals a general tendency for the USMT-4 and USMT-6 signals. However, a notable discrepancy emerges for the USMT-2 signal within the linear zone. This discrepancy can be attributed to the sensitivity of the measurement configuration, which lacks the precision to accurately quantify the difference between carriers and intermodulation products above 40 dB. For output powers below 20 dBm, the slope of the results obtained is approximately 2 dB/dB, which is consistent with the behavior of the transistor in weakly nonlinear operation.

It has been observed that the ACPR value for the USMT-4 and USMT-6 signals is lower than the C/I ratio value of the USMT-2 signal. This is due to the fact that a higher PAPR implies greater distortion. A more thorough examination can be achieved by analyzing the output spectrum at the PA output plane for the various USMT signals.

A thorough analysis of the spectrum of the USMT-2 signal at the transistor output reveals two lines corresponding to the two signal tones and two lines corresponding to the two third-order intermodulation products. In order to ensure that all signals possess equivalent power, it is imperative to calibrate the amplitudes of each carrier. To illustrate, to have the same power as a USMT-2 signal, the amplitudes of the USMT-4 signal's carriers must be reduced.

This adjustment ensures that four carriers of the USMT-4 signal attain the same power as two carriers of the USMT-2 signal. In a similar manner, the power of four third-order intermodulation products of the type $2f_i - f_j$ generated by a USMT-4 signal is equivalent to the power of two intermodulation products of the type $2f_i - f_j$ generated by a USMT-2 signal. A USMT-6 signal can be analyzed using the same approach.

The increased number of tones indicates an increase in the number of third-order intermodulation products of the type $2f_i - f_j$

Downloaded from https://www.cambridge.org/core. UNIVERSIDAD AUTONOMA METROPOLITANA, on 17 Nov 2026 at 04:20:28, subject to the Cambridge Core terms of use, available at https://www.cambridge.org/core/terms. https://doi.org/10.1017/S1759078726103699

Table 2. Number of IM_3 located in the adjacent bands of the signal, ratio between the power of the IM_3 of the USMT-N signal in relation to the USMT-2 signal, and the calculated and simulated ACPR values for an output power of 15 dBm

	$2f_i - f_j$	$f_i + f_j - f_k$	$\frac{P_{IM_3}(\text{USMT - N})}{P_{IM_3}(\text{USMT - 2})}$	ACPR/$\frac{C}{I}$ (calculated)	ACPR/$\frac{C}{I}$ (simulated)
USMT − 2	2	0	0 dB	47 dB	46.7 dB
USMT − 4	9	7	4.293 dB	42.7 dB	41.8 dB
USMT − 6	20	30	6.612 dB	40.4 dB	40.6 dB

in the adjacent bands, in addition to the additional intermodulation products of the type $f_i + f_j - f_k$, which have one-quarter of the power of the IMs in the adjacent bands of the type $2f_i - f_j$. Therefore, the relationship between the power of the IM_3s of a USMT-N signal and the power of the IM_3s of a USMT-2 signal can be calculated using equation (4). In this equation, N denotes the number of tones in the signal, R denotes the number of IMs of type $2f_i - f_j$, and S represents the number of IMs of type $f_i + f_j - f_k$. The quantities R and S depend on the number of signal carriers and the vector p_k [28, 29].

$$\frac{P_{IM_3}(\text{USMT - N})}{P_{IM_3}(\text{USMT - 2})}\ (\text{dB}) = 10 \cdot \log\left(\frac{R + \frac{1}{4}S}{N}\right) \tag{4}$$

The increase in the number of tones does not result in a significant compression of the intended signal at the output, which may be neglected since the transistor operates within its linear region.

Consequently, an increase in the number of signal tones can be interpreted as an increase in the total power of the IM_3 in the adjacent bands, while the output power of the signal remains constant. This indicates that, as the number of tones in the signal increases, ACPR decreases within the device's linear zone, as illustrated in Figure 11. Equation (5) outlines how the ACPR of a USMT-N signal is determined based on this assumption.

In this equation, $\frac{C}{I}_{\text{USMT - 2}}$ is the $\frac{C}{I}$ ratio of the USMT-2 signal, IIP3 is the third-order input intercept point, and P_{in} is the average input power.

$$\begin{aligned}\text{ACPR}\ (\text{dB}) &= \frac{C}{I}_{\text{USMT - 2}} - 10 \cdot \log\left(\frac{R + \frac{1}{4}S}{N}\right) \\ &= 2\,(\text{IIP3} - P_{in}) - 10 \cdot \log\left(\frac{R + \frac{1}{4}S}{N}\right)\end{aligned} \tag{5}$$

As illustrated in Table 2, a comparative analysis has been conducted between the ACPR for the USMT-4 and USMT-6 signals and the C/I for the USMT-2 signal. This analysis has been performed using equation (5) and the simulated values. As previously mentioned, because of the bench's sensitivity, the measured values were not used for comparison criteria.

The minor discrepancy between the calculated and measured values can be attributed to the presence of compression in the output signal and intermodulation products, which contribute to increase the ACPR value. In the nonlinear region, signal compression becomes more relevant, and the ACPR no longer follows equation (5), as can be seen in Figure 11, where the ACPR curves for the USMT-4 and USMT-6 signals converge from Pout = 19 dBm.

Conclusion

The study entailed the characterization of a pre-matched HEMT transistor utilizing USMT-2, USMT-4, and USMT-6 signals around 29 GHz. This was achieved by comparing the results obtained with measurements and simulations of figures of merit, including output power, DC drain current, PAE, and ACPR. This approach was employed to characterize the linearity of the device. The findings suggest that the device demonstrates a more pronounced decline in drain current when a USMT signal with a higher number of frequencies is applied. This phenomenon can be attributed to the effects of traps and variations in signal dynamics. A decrease in the maximum PAE value was observed with an increase in the number of tones, a phenomenon that was confirmed through both measurements and simulations. The discrepancies observed between the simulation and the measurement, such as a lower PAE value for the measurement, are attributable to the challenges in reproducing the same conditions in the simulation as in the measurement, specifically at harmonic values. The measured values are also lower than those found when characterizing the transistor alone using load-pull because the matching networks have inherent losses and are not designed to obtain maximum PAE. An analysis of the ACPR reveals a high degree of concordance between the simulation and the measurement. One noteworthy finding is that the ACPR value decreases as the number of frequencies increases. This phenomenon is caused by signal dynamics; when the signal envelope's maximum power increases, waveform distortion increases as well. Consequently, there is an increase in the number of intermodulation products in the adjacent bands.

Subsequent lines of research will entail the utilization of the USMT-8 signal for simulating the device, an examination of the NPR, and a mathematical analysis to ascertain the ACPR as a function of the number of tones in the nonlinear region. This approach will facilitate the development of a more comprehensive model. A salient point that merits attention is the necessity of conducting this comparative study using an unmatched device in accordance with the load-pull method.

Acknowledgements. The authors express their profound gratitude to United Monolithic Semiconductors for supplying the transistors that underwent characterization, as well as to the Direction Générale de l'Armement and the Centre National de la Recherche Scientifique (CNRS) for providing financial support under the GREAT Project. The experiments were carried out at the PLATINOM test facility of XLIM, a member of the CNRS RF-Net network (ANR-22-PEFT-0011).

Competing interests. The authors report no conflict of interest.

References

1. **Laurent S, Kahil SAK, Quéré R and Sombrin J** (2016) A multi-tone load pull measurement system for on-wafer characterization of microwave power transistors. In *2016 46th European Microwave Conference (EuMC)*, pp. 1119–1122. https://doi.org/10.1109/EuMC.2016.7824544

Downloaded from https://www.cambridge.org/core. UNIVERSIDAD AUTONOMA METROPOLITANA, on 17 Nov 2026 at 04:20:28, subject to the Cambridge Core terms of use, available at https://www.cambridge.org/core/terms. https://doi.org/10.1017/S1759078726103699

2. **Camarchia V, Teppati V, Corbellini S and Pirola M** (2007) Microwave measurements part II non-linear measurements. *IEEE Instrumentation & Measurement Magazine* **10**(3), 34–39. https://doi.org/10.1109/MIM.2007.4284255
3. **Teppati V, Ferrero A, Camarchia V, Neri A and Pirola M** (2008) Microwave measurements - Part III: Advanced non-linear measurements. *IEEE Instrumentation & Measurement Magazine* **11**(6), 17–22. https://doi.org/10.1109/MIM.2008.4694153
4. **Farsi S, Draxler P, Gheidi H, Nauwelaers BKJC, Asbeck P and Schreurs D** (2014) Characterization of intermodulation and memory effects using offset multisine excitation. *IEEE Transactions on Microwave Theory & Techniques* **62**(3), 645–657. https://doi.org/10.1109/TMTT.2014.2302745
5. **Angelotti AM, Gibiino GP, Florian C and Santarelli A** (2020) Broadband error vector magnitude characterization of a GaN power amplifier using a vector network analyzer. In *2020 IEEE/MTT-S International Microwave Symposium (IMS)*, pp. 747–750. https://doi.org/10.1109/IMS30576.2020.9223771
6. **Pintelon R and Schoukens J** (2012) *System Identification: A Frequency Domain Approach*. Hoboken, New Jersey: John Wiley & Sons.
7. **Verspecht J, Stav A, Teyssier J-P and Kusano S** (2019) Characterizing amplifier modulation distortion using a vector network analyzer. In *2019 93rd ARFTG Microwave Measurement Conference (ARFTG)*, pp. 1–4. https://doi.org/10.1109/ARFTG.2019.8739226
8. **Freiberger K, Enzinger H and Vogel C** (2017) SLIC EVM — Error vector magnitude without demodulation. In *2017 89th ARFTG Microwave Measurement Conference (ARFTG)*, pp. 1–4. https://doi.org/10.1109/ARFTG.2017.8000826
9. **Silva dos Santos JA, Alleman J, Reveyrand T, Medrel P, Chang C, Sommet R, Nébus JM, Prigent M and Nallatamby JC** (2025) Experimental overview of linearity metrics using complex modulated signals. *International Journal of Microwave and Wireless Technologies* **17**(7), 1097–1106. https://doi.org/10.1017/S1759078725102389
10. **Gillet V, Bouslama M, Teyssier J-P, Prigent M, Nallatamby J-C and Quéré R** (2019) An unequally spaced multi-tone load–pull characterization technique for simultaneous linearity and efficiency assessment of RF power devices. *IEEE Transactions on Microwave Theory & Techniques* **67**(7), 2505–2513. https://doi.org/10.1109/TMTT.2019.2918799
11. **Laurent S, Teyssier JP, Quere R, Sombrin J and Prigent M** (2016) Linearity characterization of RF circuits through an unequally spaced multi-tone signal. In *2016 88th ARFTG Microwave Measurement Conference (ARFTG)*, pp. 1–4. https://doi.org/10.1109/ARFTG.2016.7839729
12. **Angelotti AM and Gibiino GP** (2025) Optimal design of multisine excitations with non-overlapping intermodulation using minimal-length B_h sets. In *2025 105th ARFTG Microwave Measurement Conference (ARFTG)*, pp. 1–4. https://doi.org/10.1109/ARFTG65332.2025.11168145
13. **Sombrin JB** (2011) On the formal identity of EVM and NPR measurement methods: Conditions for identity of error vector magnitude and noise power ratio. In *2011 41st European Microwave Conference*, pp. 337–340. https://doi.org/10.23919/EuMC.2011.6101738
14. **Kester W** (2009) Noise Power Ratio (NPR)—A 65-Year Old Telephone System Specification Finds New Life in Modern Wireless Applications.
15. **Kumar R** (2016) Theoretical analysis of the noise power ratio of nonlinear power amplifiers. *Journal of Applied Mathematics* **2016**(1), 8710860. https://doi.org/10.1155/2016/8710860
16. **Freiberger K, Enzinger H and Vogel C** (2017) A noise power ratio measurement method for accurate estimation of the error vector magnitude. *IEEE Transactions on Microwave Theory & Techniques* **65**(5), 1632–1645. https://doi.org/10.1109/TMTT.2017.2654221
17. **Silva Dos Santos JA Reveyrand T, Gaillard F, Medrel P, Nebus JM, Prigent M, Nallatamby JC, Chang C** (2023) A novel fast calibration method for NVNAs based linearity setup. In *2023 International Workshop on Integrated Nonlinear Microwave and Millimetre-Wave Circuits (INMMIC)*, pp. 1–4. https://doi.org/10.1109/INMMIC57329.2023.10321796
18. **Gillet V Teyssier JP, Al Hajjar A, Gasmi A, Kacou CE, Prigent M, Quéré R** (2020) Millimeter-wave power amplifier linearity characterization using unequally spaced multi-tone stimulus. In *2020 IEEE/MTT-S International Microwave Symposium (IMS)*, pp. 755–758. https://doi.org/10.1109/IMS30576.2020.9224079
19. **Peng L, Chen J, Zhang Z and Zhang G** (2022) Design of an efficient 24–30 GHz GaN MMIC power amplifier using filter-based matching networks. *Electronics* **11**(13), 1934. https://doi.org/10.3390/electronics11131934
20. **Liu S, Ma X, Zhang Y and Xu C** (2025) Design of a high-power, high-efficiency GaN power amplifier for W-band applications. *Micromachines* **16**(9), 985. https://doi.org/10.3390/mi16090985
21. **Silva dos Santos JA, Alleman J, Leventoux M, Medrel P, Chang C, Sommet R, Courrèges F and Nallatamby JC** (2025) Measured and simulated linearity metrics comparison of a pre-matched AlGaN/GaN HEMT at 29 GHz. In *2025 20th European Microwave Integrated Circuits Conference (EuMIC)*, pp. 246–249. https://doi.org/10.23919/EuMIC65284.2025.11234497
22. **Gibiino GP, Angelotti AM, Santarelli A, Filicori F and Traverso PA** (2021). Multitone multiharmonic scattering parameters for the characterization of nonlinear networks. *IEEE Transactions on Instrumentation and Measurement* **70**, 1–12. https://doi.org/10.1109/TIM.2020.3031165
23. **ETSI** (Jun 2021) *Digital Terrestrial TV Transmitters; Harmonised Standard for Access to Radio Spectrum*.
24. **Reveyrand T, Hernandez S, Mons S and Ngoya E** (2020) SOLT and SOLR calibration methods using a single multiport 'thru' standard connection. In *2020 95th ARFTG Microwave Measurement Conference (ARFTG)*. Los Angeles, CA, USA: IEEE, pp. 1–4. https://doi.org/10.1109/ARFTG47271.2020.9241365
25. **Teyssier JP, Sombrin J, Quéré R, Laurent S and Gizard F** (2014) A test set-up for the analysis of multi-tone intermodulation in microwave devices. In *84th ARFTG Microwave Measurement Conference*, pp. 1–3. https://doi.org/10.1109/ARFTG.2014.7013408
26. **Peng LL, Canfield PC and Allstot DJ** (1992) Trap effects in p-channel GaAs MESFET's. *IEEE Transactions on Electron Devices* **39**(11), 2444–2451. https://doi.org/10.1109/16.163456
27. **Gibiino GP, Angelotti AM, Santarelli A and Florian C** (2019) Microwave characterization of trapping effects in 100-nm GaN-on-Si HEMT technology. *IEEE Microwave and Wireless Components Letters* **29**(9), 604–606. https://doi.org/10.1109/LMWC.2019.2933186
28. **Silva Dos Santos JA** (2024) Caractérisation de transistors HEMT en utilisant une méthode innovante de mesure de la linéarité. thesis, Limoges, https://theses.fr/2024LIMO0088 (accessed 28 December 2025).
29. **Gillet V** (2019) Développement d'un banc de load-pull actif innovant, utilisant un signal multi-tons large bande pour la mesure de la linéarité (EVM, NPR, ACPR) des dispositifs actifs. These de doctorat, Limoges. [Online] https://www.theses.fr/2019LIMO0114 (accessed: 22 February 2024).



José Anderson Silva dos Santos received his Engineer Degree in Electrical Engineering in 2020 from the Federal Institute of Education, Science and Technology of Paraiba in João Pessoa, Brazil, and his Ph.D. degree in electronics from University of Limoges, France in 2024. He has been a teaching assistant at the University of Limoges since 2025. His research interests encompass RF microelectronics, instrumentation, data processing, digital communications, and microwaves.



Julien Alleman received the Engineering degree in Electrical Engineering from Toulouse INP-ENSEEIHT, France, in 2022. He received the Ph.D. degree in High-Frequency Electronics from the University of Limoges, France, in 2025. He conducted his doctoral research at the XLIM Institute. His research interests focus on the application of Artificial Intelligence to RF electronics, specifically utilizing deep neural networks for the modeling and reconstruction of load-pull measurement data for GaN HEMTs.

Downloaded from https://www.cambridge.org/core. UNIVERSIDAD AUTONOMA METROPOLITANA, on 17 Nov 2026 at 04:20:28, subject to the Cambridge Core terms of use, available at https://www.cambridge.org/core/terms. https://doi.org/10.1017/S1759078726103699



Margot Leventoux received the Engineering degree in Electrical Engineering in 2023 from ENSEA, Cergy, France. She is currently pursuing the Ph.D. degree in High-Frequency Electronics at the University of Limoges, France, since 2024. She conducts her doctoral research at the XLIM Institute. Her research interests include passive and active load-pull transistor measurements, as well as instrumentation and data processing.



Pierre Medrel received the Ph.D. degree in electronics from the University of Limoges, France, in 2014. From 2014 to 2015, he was a postdoctoral Scientist at the IMS laboratory, Bordeaux, France. He is now an associate professor with the XLIM institute, Limoges. His main field of interest is high-efficiency microwave PA architectures and non-linear device characterization.



Christophe Chang received the Ph.D. degree, under the Joint Doctoral Degree Program, from the XLIM Laboratory, University of Limoges, Limoges, France, and Thales Airborne Systems, Trappes, France. In 2004, he joined the XLIM Laboratory, University of Limoges, as a Post-Doctoral Researcher. He was involved in the characterization and the nonlinear modeling of the UMS GaInP/GaAs bipolar transistor. In 2005, he joined UMS SAS, where he is currently a Senior Modeling Engineer supporting the development of AsGa-based pHEMT power technologies such as PPH25X and PPH15X (technology support, characterization, and modeling). Since 2007, he has been involved in the support of the development of UMS GaN based technologies (characterization and nonlinear model building). He has participated in the development and the qualification of the 0.25 µm GH25 technology. Since 2014, he has been involved in the 0.15 µm GH15 technology development.



Fabien Courrèges received the B.S. degree in fundamental physics of the University of Orleans (France) in 1999, the M.S. degree in robotics of the University of Poitiers (France) in 2000 and the PhD degree in signal processing, robotics, and control at the University of Orl´eans in 2003. He is tenured assistant professor with the Intelligent Systems and Networks department of the XLIM research institute from the University of Limoges (France) since 2007. His main research concern is about systems and data modeling and processing for enabling design and control of smart and autonomous plants and systems.



Raphaël Sommet received the French aggregation degree in applied physics and the Ph.D. degree from the University of Limoges, Limoges, France, in 1991 and 1996, respectively. Since 1997, he has been a Permanent Researcher at XLIM, Institut de Recherche, Unités Mixtes de Recherche Centre National de la Recherche Scientifique 6172, Faculté des Sciences et Techniques, Université de Limoges, in the C2S2 team "Nonlinear Microwave Circuits and Subsystems." His research interests concern heterojunction-bipolar-transistor device simulation, 3-D thermal finite element simulation, model order reduction, microwave circuit simulation, and generally the coupling of all physics-based simulation with circuit simulation.



Jean-Christophe Nallatamby received the Ph.D. degree in electronics from the University of Limoges, Limoges, France, in 1992. He is currently a Professor with the University of Limoges. His current research interests include the microwave, low-frequency noise characterization and modeling of high-speed semiconductor devices, characterization of charge-trapping effects in GaN HEMTs, and understanding its physical behavior using TCAD-based device simulation.

Downloaded from https://www.cambridge.org/core. UNIVERSIDAD AUTONOMA METROPOLITANA, on 17 Nov 2026 at 04:20:28, subject to the Cambridge Core terms of use, available at https://www.cambridge.org/core/terms. https://doi.org/10.1017/S1759078726103699